SUPPORTING INFORMATION FOR:

Biotransformation of Two Pharmaceuticals by the Ammonia-Oxidizing Archaeon
Nitrososphaera gargensis

Yujie Men,[*,†,‡] Ping Han,[§] Damian E. Helbling,[‖] Nico Jehmlich,[⊥] Craig Herbold,[§] Rebekka Gulde,[†]

Annalisa Onnis-Hayden,[#] April Z. Gu,[#] David R. Johnson,[†] Michael Wagner,[§] and Kathrin Fenner[†,⊗]

[†]Eawag, Swiss Federal Institute of Aquatic Science and Technology, 8600 Dübendorf, Switzerland

[‡]Department of Civil and Environmental Engineering, University of Illinois at Urbana−Champaign, Urbana, Illinois 61801, United States

[§]Department of Microbiology and Ecosystem Science, Division of Microbial Ecology, Research Network "Chemistry meets Microbiology", University of Vienna, Althanstrasse 14, 1090 Vienna, Austria

[‖]School of Civil and Environmental Engineering, Cornell University, Ithaca, New York 14853, United States

[⊥]Department of Proteomics, Helmholtz-Centre for Environmental Research − UFZ, 04318 Leipzig, Germany

[#]Department of Civil and Environmental Engineering, Northeastern University, Boston, Massachusetts 02115, United States

[⊗]Department of Environmental Systems Science, ETH Zürich, 8092 Zürich, Switzerland

*Corresponding author:

Yujie Men

Department of Civil and Environmental Engineering

University of Illinois at Urbana-Champaign,

Address: 3209 Newmark Civil Engineering Laboratory, MC-250

205 North Mathews Ave.

Urbana, IL 61801-2352, USA

Email: ymen2@illinois.edu

Phone: (217) 244-8259

Table of Contents

List of Figures

List of Tables

S1 Analytical analysis using LC-MS/MS

MPs and target transformation products (TPs) (Table S1) in culture supernatant were first cleaned by automated online SPE, and then analyzed using reversed-phase liquid chromatography coupled to a high-resolution quadrupole orbitrap mass spectrometer (QExactive, Thermo Scientific). The online-SPE procedure involved three steps: loading, enrichment, and elution as described previously.[1] In detail, 20 mL diluted sample or standard with internal standard mix-stock (200 µL sample or standard + 100 µL of µg/L internal standard mix-stock + 19.7 mL nanopure water) was loaded with two times of 10 mL via a dispenser syringe. A self-made mixed-bed multilayer extraction cartridge and two six-port valves were used for sample enrichment. The SPE cartridge was prepared in-house by filling an empty cartridge (stainless steel, 20 mm × 2.1 mm, BGB Analytik AG, Germany) with 8 mg Oasis HLB (15 µm, Waters) as first material in enrichment flow direction. As second material, 11 mg of a mixture of Strata X-AW (33 µm), Strata X-CW (25 µm, both from Phenomenex, Brechbühler AG, Schlieren, Switzerland) and Isolute ENV+ (70 µm, Biotage, Uppsala, Sweden) in a ratio of 1/1/1.5 (X-

AW/X-CW/ENV+) was used. One SPE cartridge was used for up to 200 injections, *i.e.* one SPE cartridge per measurement sequence. The sample was loaded with a flow rate of 2 mL/min and subsequently eluted in back-flush mode with methanol containing 0.1% formic acid at a flow rate of 30 μL/min for 7 min. The acidic methanol SPE eluate was then diluted with water (HPLC grade) containing 5 mM ammonium acetate by an additional pump with an active mixer (Portmann Instruments AG, Biel, Switzerland) with a low-volume (15 μL) mixing chamber. This procedure enables the refocusing of the eluted analytes on the analytical column. For HPLC, a mobile phase consisting of nanopure water (Barnstead Nanopure, Thermo Scientific) and methanol (HPLC-grade, Fisher Scientific) both augmented with 0.1% formic acid (98-100%, Merck) at a flow rate of 300 μL/min was used. The initial gradient (90:10 water/methanol) was held for 4 min, then increased to 10:90 water/methanol over 16 min, held for 6 min. It was then set back to the initial gradient over 0.2 min, held for 6 min for column conditioning before the next analysis. The total run time for one sample including online SPE and LC-MS/MS was 32 min. Detection with the mass spectrometer was done in positive ionization mode. Electrospray ionization was triggered at a capillary temperature of 350°C and a spray voltage of 4 kV. A mass calibration and mass accuracy check was carried out prior to the measurement with an in-house amino acid solution, which enhanced calibration for small masses. Mass accuracy was always better than 1.5 ppm. The compounds were measured in full-scan mode at a resolution of 140,000 at 200 *m/z* and a scan range of 100-550 *m/z*. Three data-dependent MS/MS were triggered after each full-scan with a resolution of 17500 at 200 *m/z*. The calibration curve over a range between 10 and 750 ng/L in 20 mL with seven calibration points was measured prior to the sample series of the corresponding experiments. The internal standards (400 ng/L) used for the quantification of MPs and TPs are listed in Table S2. For the compounds whose isotopically labeled internal

standards were not available, structurally similar internal standards with close retention times were used instead. The lowest concentration used for the calibration curve (*i.e.* 10 ng/L) was considered as the limit of quantification (LOQ). To elucidate structures of all identified TP peaks from suspect and nontarget screening, additional MS^2 measurements were conducted later with a Q Exactive instrument (Thermo Scientific). In individual runs for each TP, 6 targeted MS^2 scans were triggered after each full scan in positive-ionization mode with normalized collision energies of 15, 30, 45, 60, 75, and 90 (dimensionless).

Table S1. List of the ten tested compounds, selected transformation products (TPs) and analogous compounds

Group	Compound	Acronym	Formula	Structure	Category
Phenyl urea	Isoproturon	ISO	$C_{12}H_{18}N_2O$		Herbicide
	Diuron	DIU	$C_9H_{10}Cl_2N_2O$		Herbicide
	Chlortoluron	CHL	$C_{10}H_{13}ClN_2O$		Herbicide
Tertiary amide	Valsartan	VAL	$C_{24}H_{29}N_5O_3$		Pharmaceutical
	DEET	DEET	$C_{12}H_{17}NO$		Insect repellent
	Napropamide	NAP	$C_{17}H_{21}NO_2$		Herbicide
Tertiary amine	Venlafaxine	VEN	$C_{17}H_{27}NO_2$		Pharmaceutical
	Mianserin	MIA	$C_{18}H_{20}N_2$		Pharmaceutical
	Pheniramine	PHE	$C_{16}H_{20}N_2$		Pharmaceutical
	Ranitidine	RAN	$C_{13}H_{22}N_4O_3S$		Pharmaceutical
	Mianserin N-oxide	MIA N-oxide	$C_{18}H_{20}N_2O$		Suspected TP of MIA
	Desmethyl-mianserin	NorMIA	$C_{17}H_{18}N_2$		Suspected TP of MIA

S5
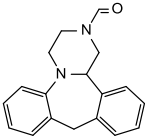
Normianserin formamide	NorMIA formamide	$C_{18}H_{18}N_2O$		Suspected TP of MIA
Ranitidine *S*-oxide	RAN *S*-oxide	$C_{13}H_{22}N_4O_4S$		Suspected TP of RAN
Ranitidine *N*-oxide	RAN *N*-oxide	$C_{13}H_{22}N_4O_4S$		Suspected TP of RAN
Mirtazapine	MIR	$C_{17}H_{19}N_3$		MIA analogue
1-oxo mirtazapine	1-oxo MIR	$C_{17}H_{17}N_3O$		1-oxo MIA analogue

Table S2. Internal standards used for the quantification of MPs and TPs

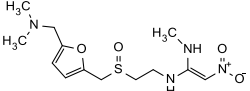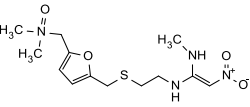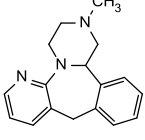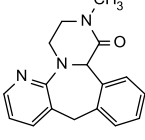| Compound	Retention Time (min)	Internal Standard	RT for InStd (min)
Isoproturon	13.4	Isoproturon-D6	13.4
Diuron	13.6	Diuron-D6	13.5
Chlortoluron	12.8	Chlortoluron-D6	12.7
Valsartan	15.5	Valsartan-13C5,15N	15.5
DEET	13.3	DEET-D10	13.3
Napropamide	15.9	Valsartan-13C5,15N	15.5
Venlafaxine	10.9	Venlafaxine-D6	10.9
Mianserin	12.0	Venlafaxine-D6	10.9
Pheniramine	8.1	Fluconazol-D4	8.1
Ranitidine	3.8	Ranitidine-D6	3.8
Mianserin *N*-oxide	12.8	Venlafaxine-D6	10.9
Desmethylmianserin	12.4	Venlafaxine-D6	10.9
1-oxo mianserin	14.3	Venlafaxine-D6	10.9
Ranitidine *S*-oxide	2.3	Ranitidine-D6	3.7
Ranitidine *N*-oxide	4.1	Ranitidine-D6	3.7

S2 Sorption and abiotic biotransformation experiments

In order to evaluate the sorption effects of $CaCO_3$ precipitates in the medium matrix and abiotic degradation of MP, the same setup as the biotransformation experiment described in the main text was carried out without the addition of AOM biomass. Fresh medium (autoclaved) with and without $CaCO_3$ precipitates were used for comparison. The concentration difference between 2h samples taken from medium with $CaCO_3$ and 0h samples from medium without $CaCO_3$ was considered as removal caused by sorption. No significant sorption in the $CaCO_3$-containing medium was observed for the nine tested MPs (Figure S1). The abiotic degradation in autoclaved fresh medium without cells was 10–22% for NAP, MIA and PHE, and less than 5% for the other MPs.
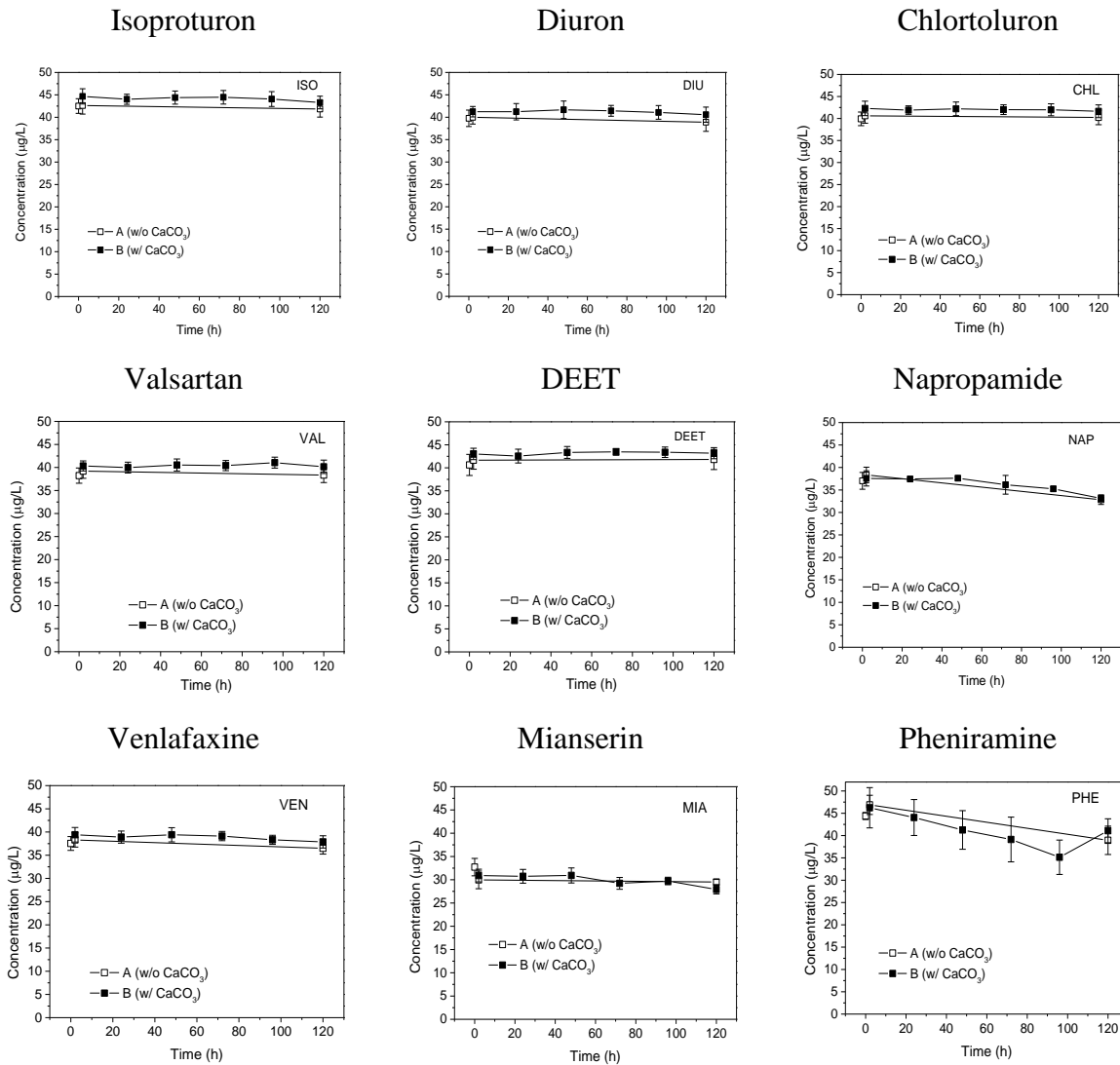
Figure S1. Sorption effects of MPs in fresh medium containing $CaCO_3$ precipitates in comparison to medium without $CaCO_3$ precipitates.
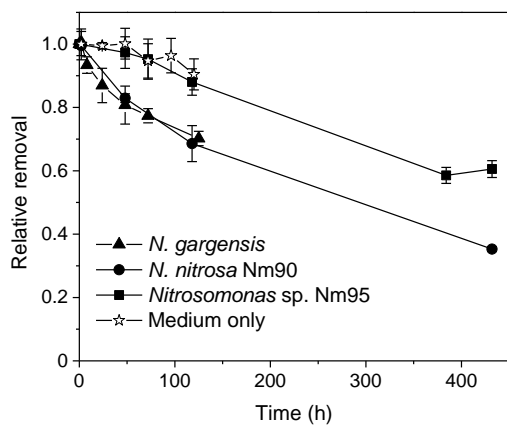
Figure S2. Comparison of mianserin removal in medium containing heat-inactivated biomass of the three AOM strains (MP removal in autoclaved cell-free fresh medium is included for comparison).
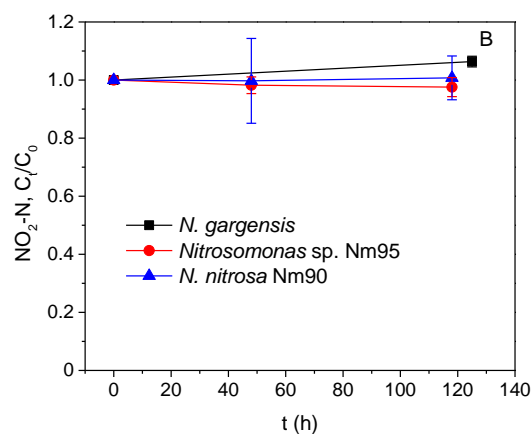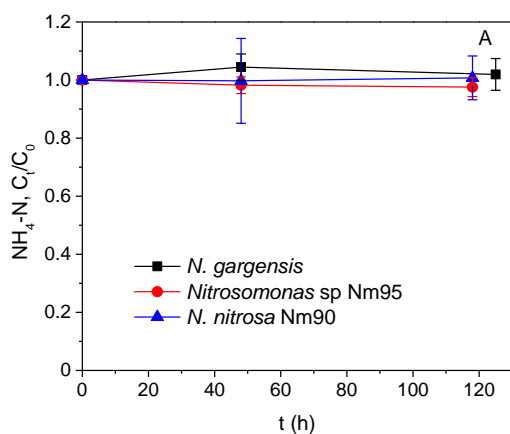
Figure S3. Relative ammonia removal (A) and nitrite formation (B) in heat-inactivated biomass of the AOA and AOB strains.

S3 MP Biotransformation by *N. gargensis*, *N. nitrosa* Nm90 and and *Nitrosomonas* sp. Nm95

MP biotransformation activities were only observed for MIA and RAN for the AOA and AOB strains tested in this study. For the rest eight MPs, the MP concentrations during a 5-day incubation, in comparison with those in the control experiment with heat-inactivated biomass are shown in Figure S4-S6, for *N. gargensis*, Nm90 and Nm95, respectively.
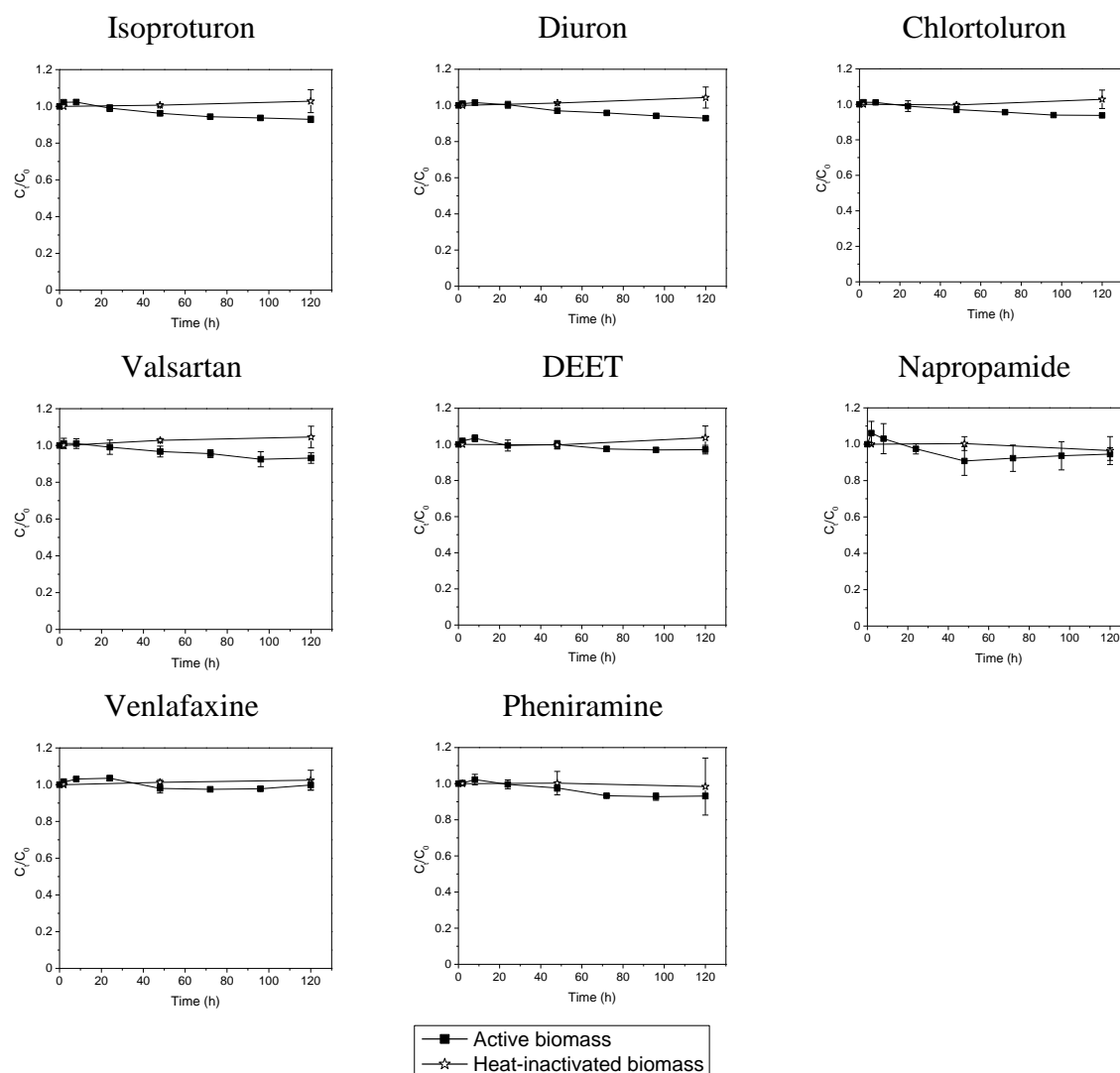
Figure S4. Biotransformation of the other eight MPs by *N. gargensis*.
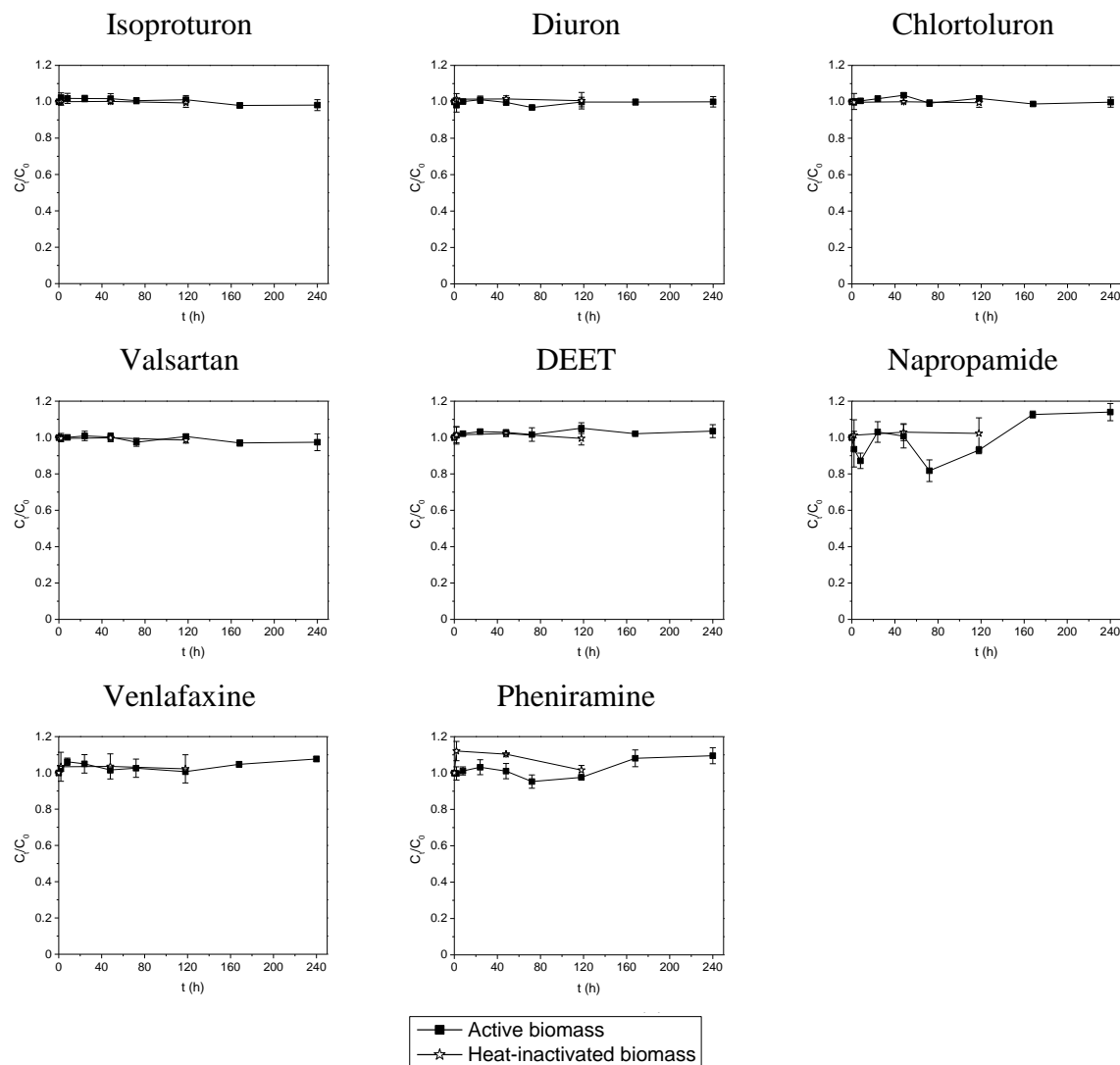
Figure S5. Biotransformation of the other eight MPs by the AOB *N. nitrosa* Nm90.
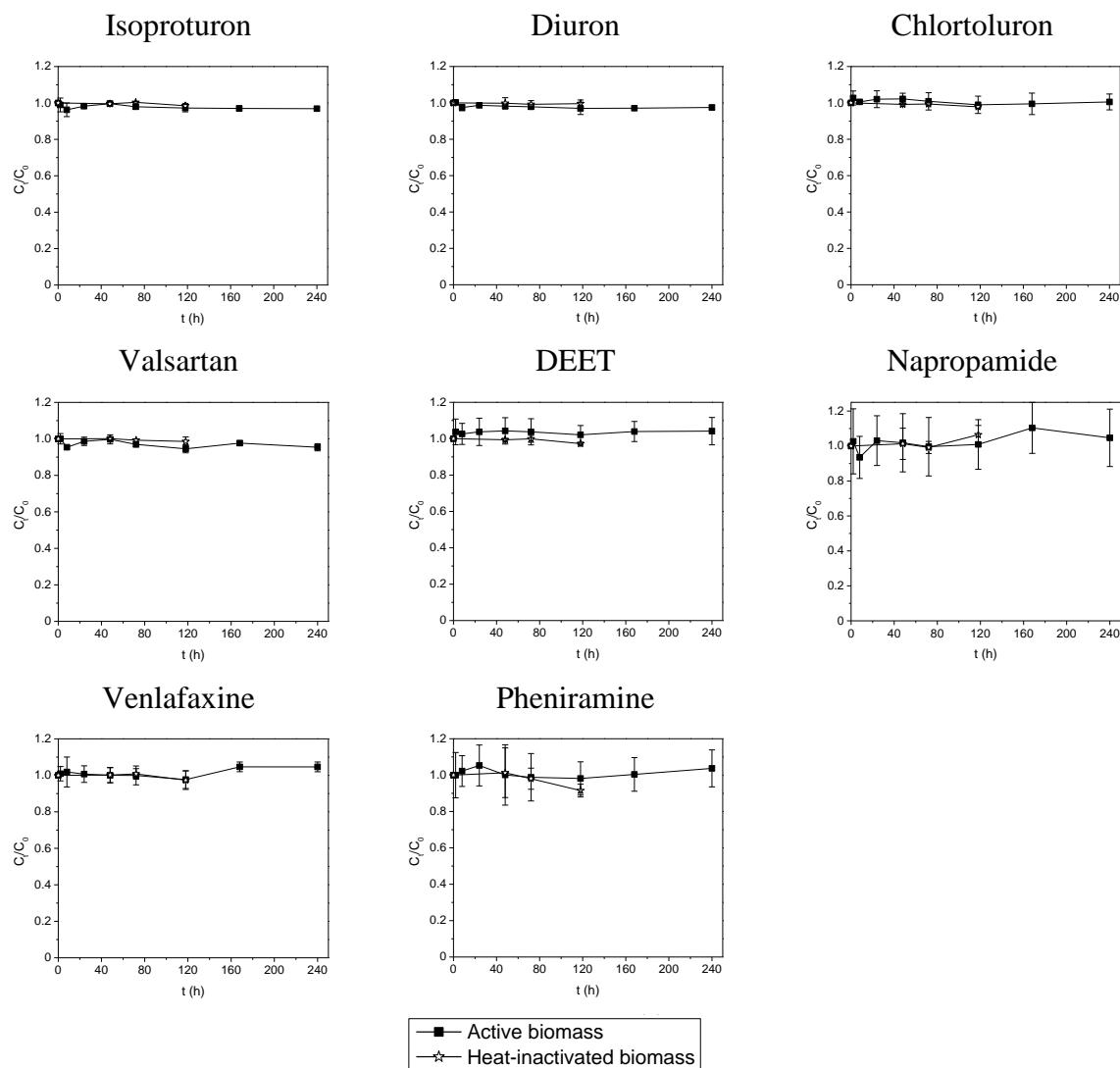
Figure S6. Biotransformation of the other eight MPs by the AOB *Nitrosomonas* sp. Nm95.

S4 Estimation of first-order kinetics parameters

To compare biotransformation activities among different biological samples, we considered

several existing cometabolic models[2, 3]. We found the reductant model and the competition model

suitable for MIA- and RAN-added cultures, respectively (see equations in Table S3).

Table S3 Cometabolic model equations

Model	Growth substrate	Cometabolic (Non-growth) substrate
First-order model[3]	$\dfrac{dS_g}{dt} = -\dfrac{k_g X S_g}{K_g + S_g}$	$\dfrac{dS_c}{dt} = -k_c X S_c$

Reductant model[3] (MIA)	$\dfrac{dS_g}{dt} = -\dfrac{k_g X S_g}{K_g + S_g}$	$\dfrac{dS_c}{dt} = -\dfrac{k_c X S_c}{K_c + S_c}\dfrac{S_g}{K_g + S_g}$
Competition[2, 3] model (RAN)	$\dfrac{dS_g}{dt} = -\dfrac{(k_g - k_{inact}S_c) X S_g}{K_g(1 + \frac{S_c}{K_c}) + S_g}$	$\dfrac{dS_c}{dt} = -\dfrac{(k_c - k_{inact}S_c) X S_c}{K_c(1 + \frac{S_g}{K_g}) + S_c}\dfrac{S_g}{K_g + S_g}$

Where, S_g and S_c are the concentration of growth substrate (NH_3 or the corresponding product NO_2^-) and cometabolic substrate (MIA or RAN), respectively; k_g and k_c are the specific maximum utilization rates, K_g and K_c are the half-saturation constants for growth substrate and cometabolic substrate, respectively; k_{inact} is the specific inactivation coefficient of RAN on ammonia monooxygenases; the recovery effect of the inhibited enzyme is neglected (as little inhibition on RAN biotransformation, the enzyme inactivation effect can be neglected in the cometabolic substrate equation); X is biomass concentration.

In this study, ammonium was provided as unlimited substrate ($S_g \gg K_g$) by semi-continuous addition, except for the minimal ammonium samples (Lo_NH4), and we observed a nearly constant ammonium turnover rate without decrease for both MIA and RAN (Fig 3B). Given that, the dependence of MP concentration on ammonia concentration in the reductant and inhibition models can be neglected over the entire time course, if we assume $K_c \gg S_c$ or $K_c \left(1 + \dfrac{S_g}{K_g}\right) \gg S_c$, it is thus simplified as first-order model. Therefore, a first-order model describing the contribution of all three processes to the observed decrease of the aqueous concentration of individual MPs was adopted as described previously[4, 5], as well as in the main text. The fitting quality was evaluated by plotting measured data against model predictions including 90% credibility intervals and by the root-mean square errors (Fig. S7).
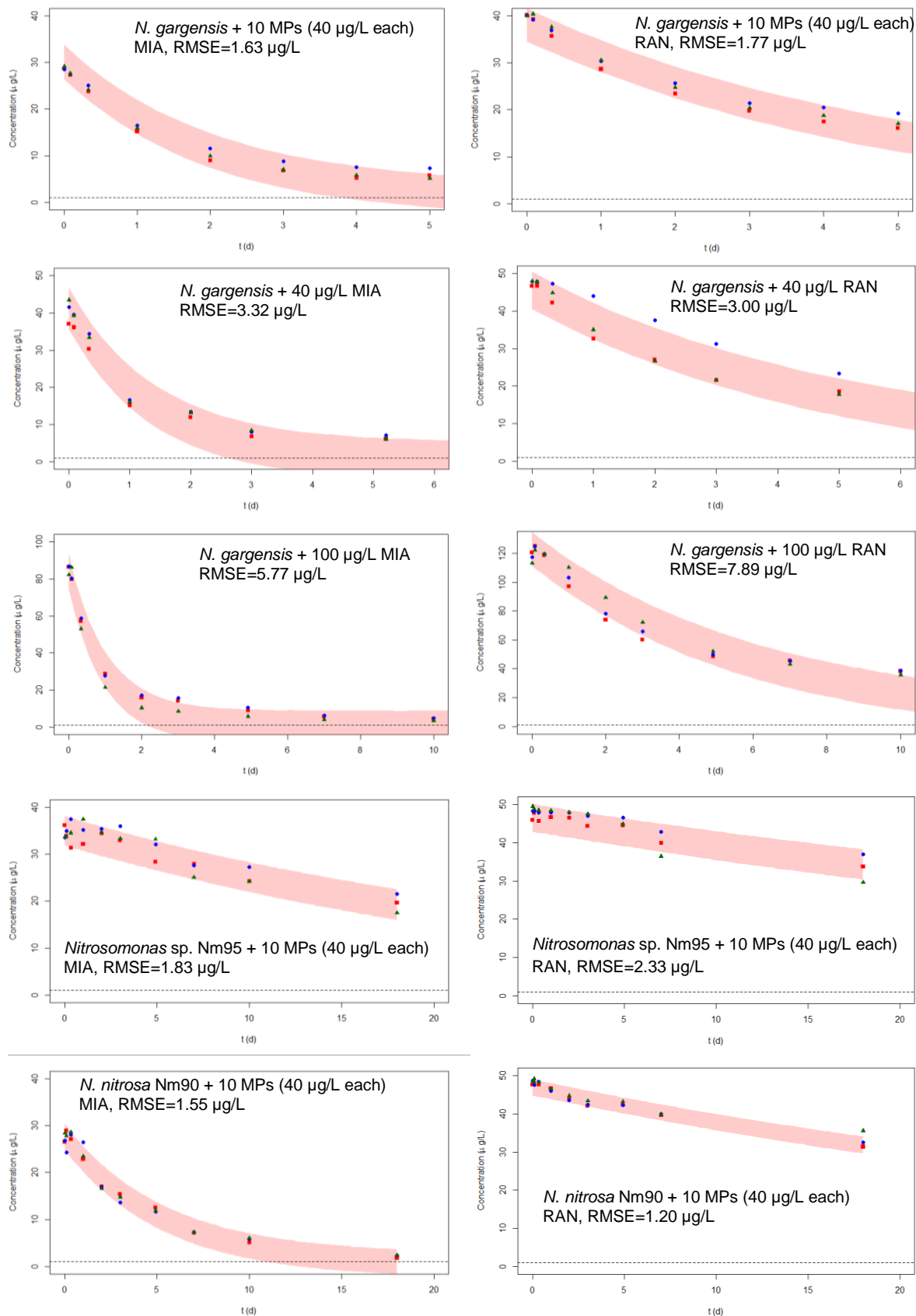
Figure S7. Model fitting plot with root-mean square errors (RMSE) of the pseudo first-order modelling (shaded areas are the 90% credibility intervals of the model fit to the measured data; red square, blue dot and green triangle represent three biological replicates).

S5 Biotransformation of RAN *S*-oxide and RAN *N*-oxide by *N. gargensis*

The two known RAN TPs, RAN *S*- and *N*-oxide were only detected in concentrations that accounted for less than 1% of the total RAN added, and no other suspected TPs were identified using suspect screening. One possible reason could be that RAN *S*- or *N*- oxide were indeed the primary TPs, but were not detected at high concentrations because they were rapidly further biotransformed. To test this hypothesis, we compared RAN *S*-, *N*-oxide and RAN biotransformation by the same amount *N. gargensis* pure culture. The experimental setup was the same as described in the main text. RAN, RAN *S*-, or *N*-oxide (40 µg/L) was added separately into the culture bottles before the inoculation of *N. gargensis*. RAN *S*- and *N*- oxide were biotransformed at a similar rate as RAN by *N. gargensis* (Figure S7). Based on kinetic principles, an accumulation of RAN *S*- or *N*-oxide would be expected if either of them was formed as the sole TP from RAN, which was not observed in our study. Therefore, other TPs must be formed during RAN biotransformation.
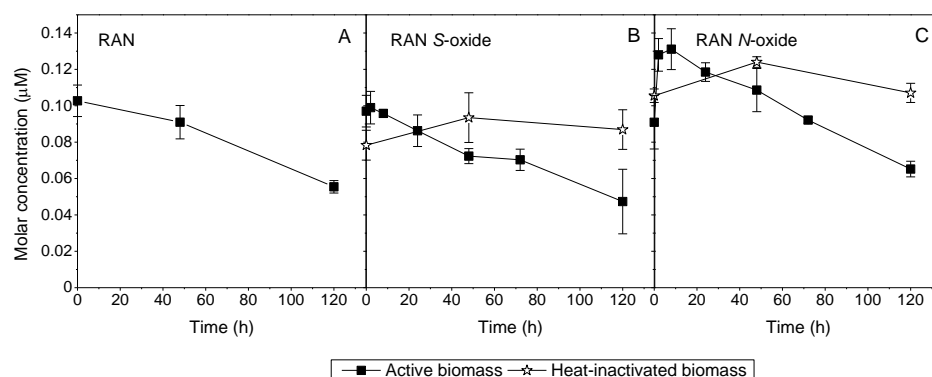

Figure S8. Biotransformation of RAN (A), RAN *S*-oxide (B) and RAN *N*-oxide (C) by *N. gargensis*.

S6 Structure elucidation of MIA TP279, RAN TP273, TP289 and TP303

There are five tentative structures for TP279 (Figure S9A). First, normianserin formamide was excluded because a reference compound of normianserin formamide that was chemically synthesized by Samuel Derrer (Eawag, Switzerland) and NMR-confirmed by Daniel Rentsch (Empa, Switzerland) had a different retention time (15.8 min) from TP279 (14.3 min), as well as different MS^2 spectra (Figure S10A&D). Therefore, TP279 should be one of the four oxo MIA structures. We assumed that MIA TP279 should share similar MS^2 fragments with its corresponding oxo MIR analogue, as we observed for MIA and its analogue MIR that fragment pairs (*i.e. m/z* 234/235, 222/223, 208/209, the mass difference was due to the change from 6-C in MIA to 6-N in MIR) were detected (Figure S10E&F). Since 10-oxo MIR had a completely different fragmentation from TP279, the 10-oxo MIA structure is excluded (Figure S10C). According to the MS^2 spectra of TP279, *m/z* 58 (C_3H_8N) was highly likely formed from the upper aliphatic ring (1-, 3-, 4-C and 2-N), given that the fragment with intact aromatic ring structure (*m/z* 194) was detected instead of fragments with open lower rings (Figure S10A). If this was the case, the fragment *m/z* 58 could not be formed for 3-oxo MIA. Both 1- and 4-oxo MIA structures agreed with the MS^2 fragments observed for TP279. If it was 4-oxo MIA, *m/z* 58 would be formed by breaking the C-C bond that connects 1- and 14b-C, instead of the C-N bond between 4-C and 5-N in 1-oxo MIA, which is less likely. We further did MS^3 analysis on two selected O-containing fragments (*m/z* 236 and 222, Figure S10A and Table S3) from MS^2 spectra on Orbitrap XL (Thermo Scientific), trying to identify the oxo position. However, the product ions detected from MS^3, which were consistent as observed from MS^2, did not provide more evidence to differentiate 1-oxo MIA from 4-oxo MIA. In addition, we analyzed the MS^2 spectra of 1-oxo MIR to find unique fragments that can help the identification. The results showed three major fragments in common with TP279 (*i.e. m/z* 58, *m/z* 251/252, and *m/z* 194/195) (Figure S10B),

none of which can be used for further differentiation. A comparison with MS^2/MS^3 spectra of 3-
and 4-oxo MIR (not currently available) may be needed to determine the exact structure of TP279.
Altogether, we here conclude that TP279 is an oxo MIA with the oxo group at α-C position (the
C next to the N of a tertiary amine group, *i.e.* 1-, 4-, or 3-C), designated as "α-oxo MIA". We
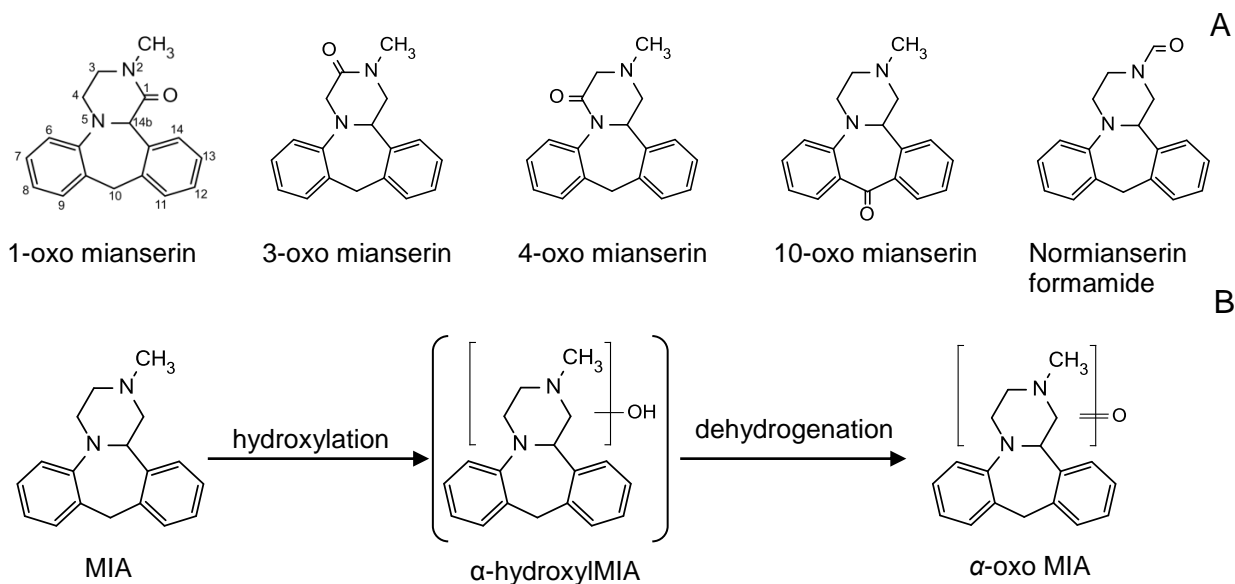propose a likelihood order of 1-oxo MIA > 4-oxo MIA > 3-oxo MIA.

Figure S9. Possible structures of MIA TP279 (A) and proposed formation pathways (B).
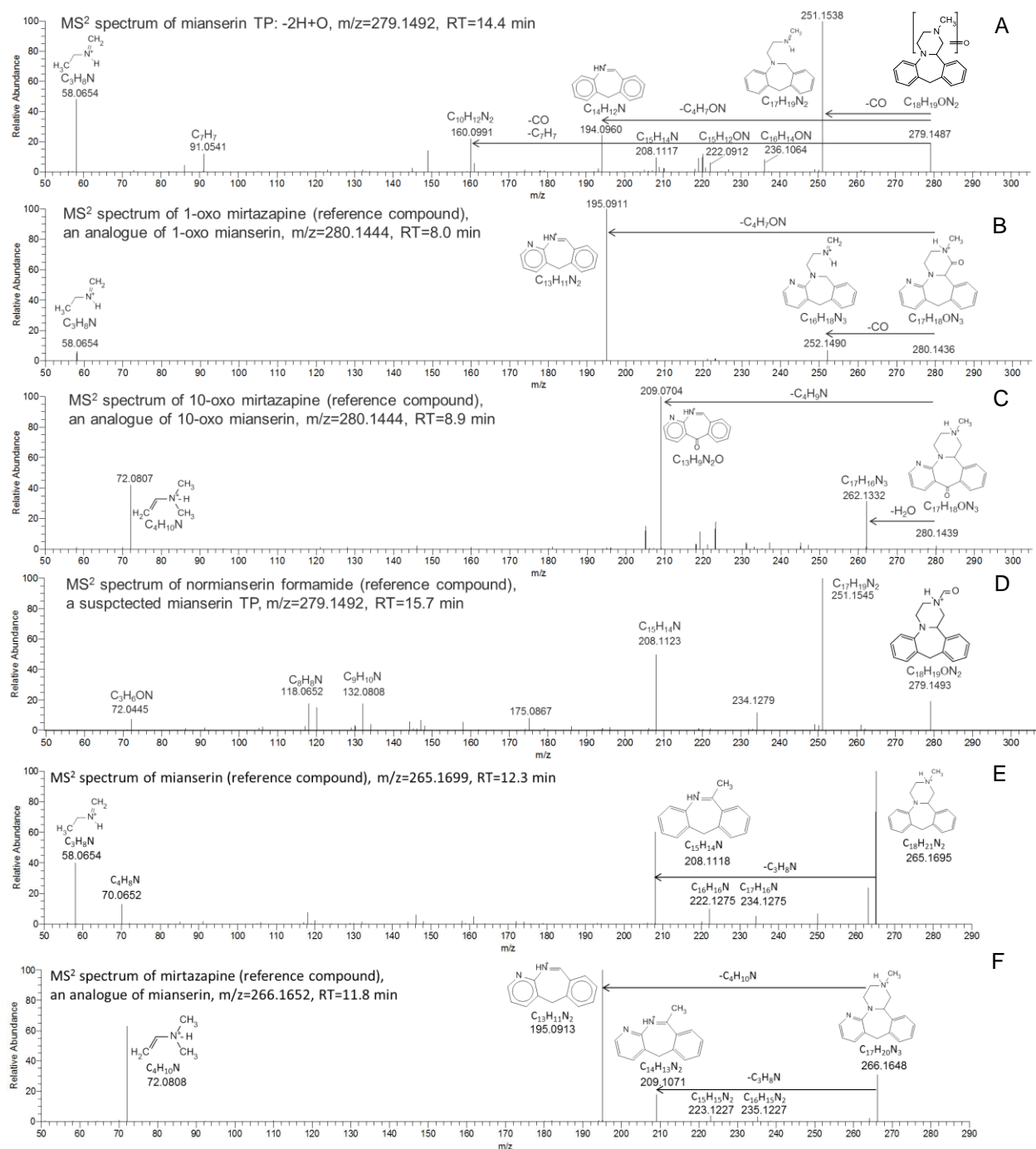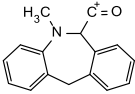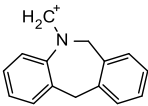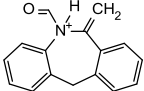
Figure S10. MS^2 spectra of TP279 (A), 1-oxo MIR (1-oxo MIA analogue) (B), 1-oxo MIR (10-oxo MIA analogue) (C), normianserin formamide (another possible structure of TP279) (D), MIA (E), and MIR (F); Note: the structures corresponding to different fragments are the most likely ones, we acknowledge that other structures may also apply.

Table S4. MS^3 analysis on two selected O-containing MS^2 fragments of TP279
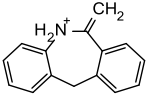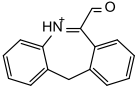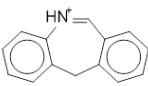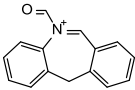
MS^2 product ion as MS^3 precursor ion, m/z (formula)	Possible structure	MS^3 product ion m/z (formula)	Possible structure	Leaving group
236.1067 (C$_{16}$H$_{14}$ON)	(for 1-oxo MIA) (for 4-oxo MIA)	208.1117 (C$_{15}$H$_{14}$N)	(for 1-oxo MIA) (for 4-oxo MIA)	CO
222.0910 (C$_{15}$H$_{12}$ON)	(for 1-oxo MIA) (for 4-oxo MIA)	194.0958 (C$_{14}$H$_{12}$N)		CO

Structures of RAN TP273, TP289, and TP303 were also elucidated from MS^2 spectra. The chromatogram, MS and MS^2 spectra, formula, proposed structure, as well as structure interpretation for each of the three TPs are included in Fig. S11. A biotransformation pathway is proposed accordingly as shown in Fig. S12, which can occur biologically. The formula and structures of the intermediates present no conflict with MS^2 fragments in Figure S11.

Name   RAN_TP_273.1263_3.2

Chromatogram
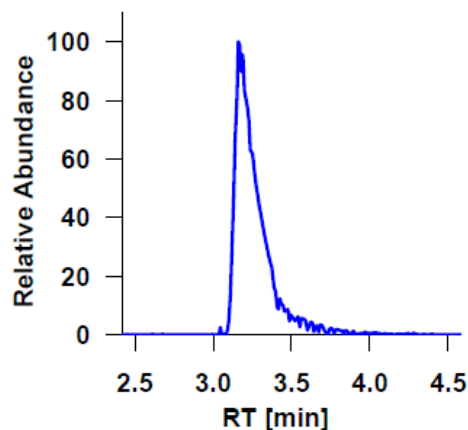
MS Spectra

MS² Spectra

Formula
$C_{12}H_{20}N_2SO_3$

Atomic Modification
$-CH_2N_2$

Proposed Structure
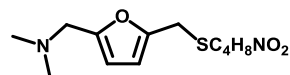
Confidence Level
Level 3
TP class

Additional Evidence for Structure Interpretation

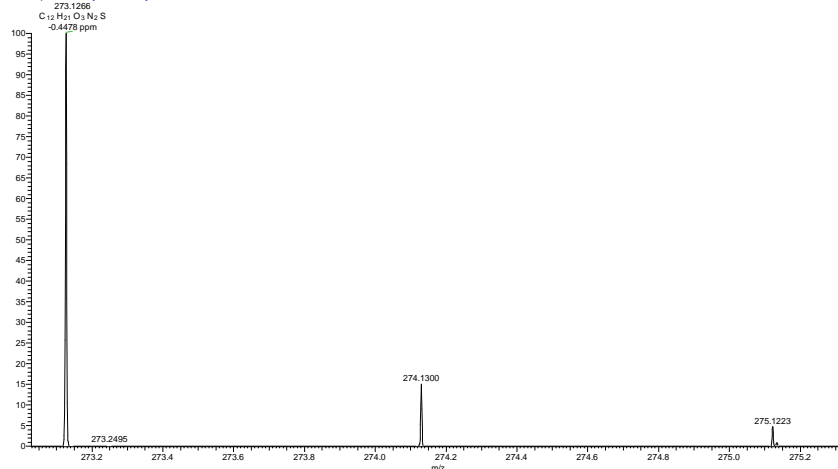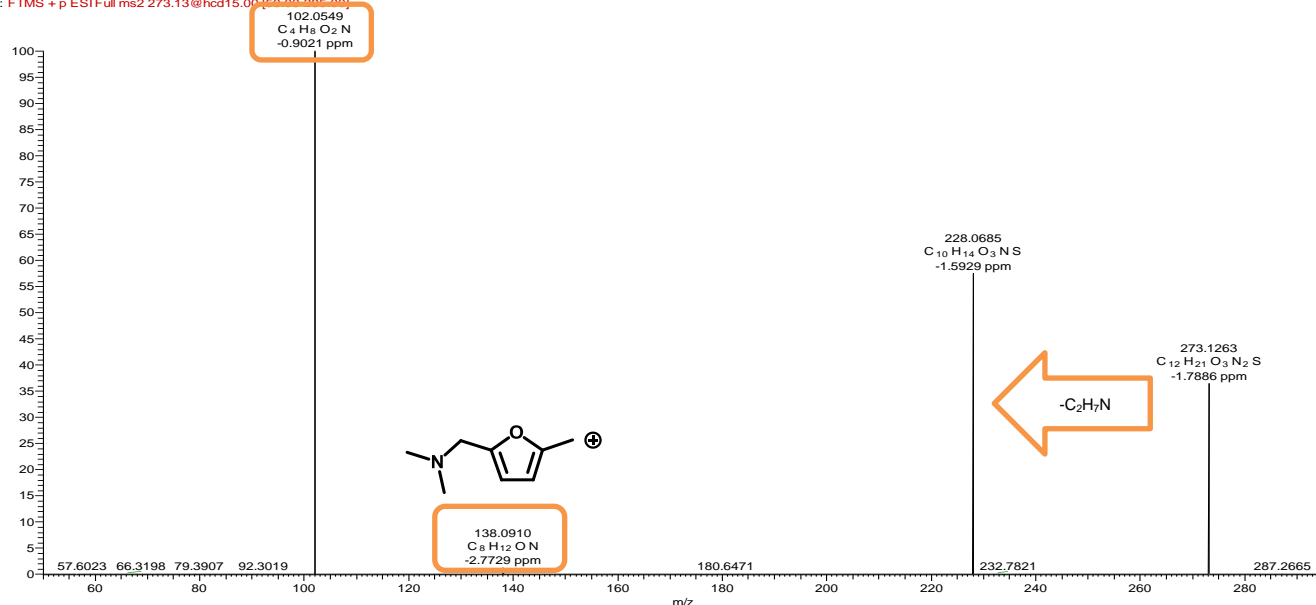The MS² fragment at the nominal mass 138 as well as the neutral loss of C_2H_7N was observed for RAN, indicating that the substructure shown at nominal mass 138 is also a part of this TP. The MS² fragment at the nominal mass 102 indicates that the remaining atoms are connected. In the MS² spectrum at a collision energy of 60, an MS² fragment was observed at the exact mass of [M+H] at 134.0269 ($C_4H_8O_2NS$, $\Delta m/z$=-0.8150ppm) indicating that the remaining part is connected to the sulfur atom. In the MS² spectrum measured at a collision energy of 90 an MS² fragment was observed at [M+H] at 72.0444 (C_3H_6ON, $\Delta m/z$=-0.3533ppm), which most likely belongs to the undefined part. The neutral loss between the MS² fragment at the nominal mass 102 and 72 is CH_2O. This indicates that the undefined part of $C_4H_8NO_2$ can be fragmented into two parts consisting of C_3H_6ON and CH_2O. The detailed structure of the remaining part, however, remains unknown.

Attributed Reaction from the Parent Compound to this TP

It was not possible to assign a reaction to this parent TP pair.

S20

Name RAN_TP_289.1212_3.2

Chromatogram

**MS Spectra**
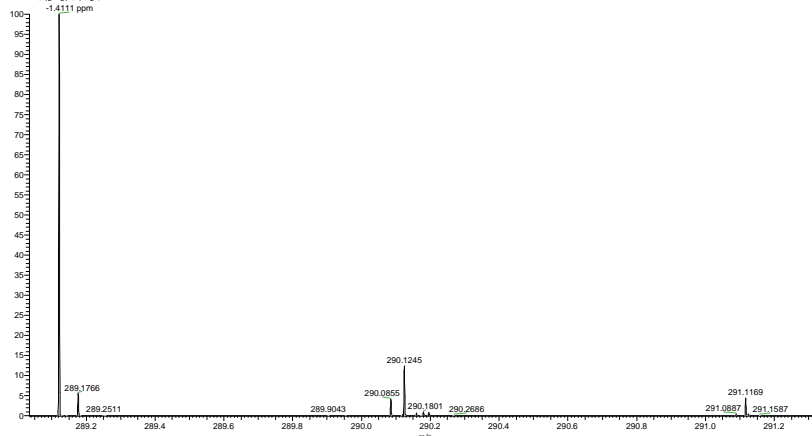
MS² Spectra

Formula
$C_{12}H_{20}N_2SO_4$

Atomic Modification
$-CH_2N_2$ +O

Proposed Structure

Confidence Level
Level 3
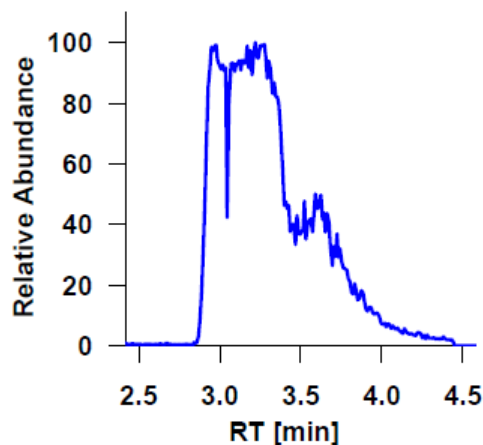TP class

Additional Evidence for Structure Interpretation

The MS² fragment at the nominal mass 138 as well as the neutral loss of C_2H_7N was observed for RAN as well as for the RAN_TP_273.1263_3.2 and indicate that the substructure shown at nominal mass 138 is also a part of this TP. The MS² fragment at the nominal mass 118 indicates that the remaining atoms are connected. The structural evidence for this TP are similar to the ones for RAN_TP_273.1263_3.2, except that this TP consists of one extra oxygen atom and that a neutral loss of H_2O can be observed multiple times. The occurrence of this neutral loss between the MS² fragments with the nominal mass 118 and 100 indicates that a hydroxyl moiety might be present in the remaining, undefined part of the molecule. The MS² fragment at the nominal mass 72 belongs most likely to the undefined part and was also observed for RAN_TP_273.1263_3.2. The neutral loss between the MS² fragment at the nominal mass 118 and 72 is CH_2O_2. This indicates that the undefined part of $C_4H_8NO_3$ can be fragmented into two parts consisting of C_3H_6ON and CH_2O_2. The detailed structure of the remaining part, however, remains unknown.

Attributed Reaction from the Parent Compound to this TP

It was not possible to assign a reaction to this parent TP pair.
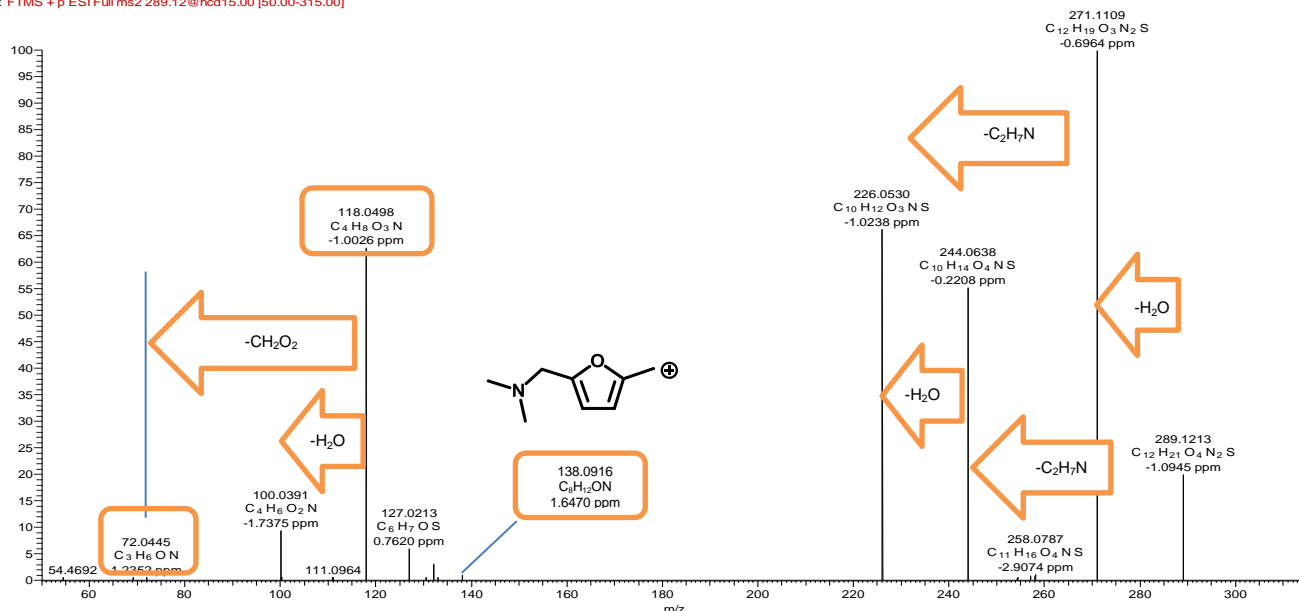
Name   RAN_TP_303.1367_3.7

Chromatogram

MS Spectra
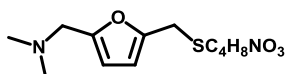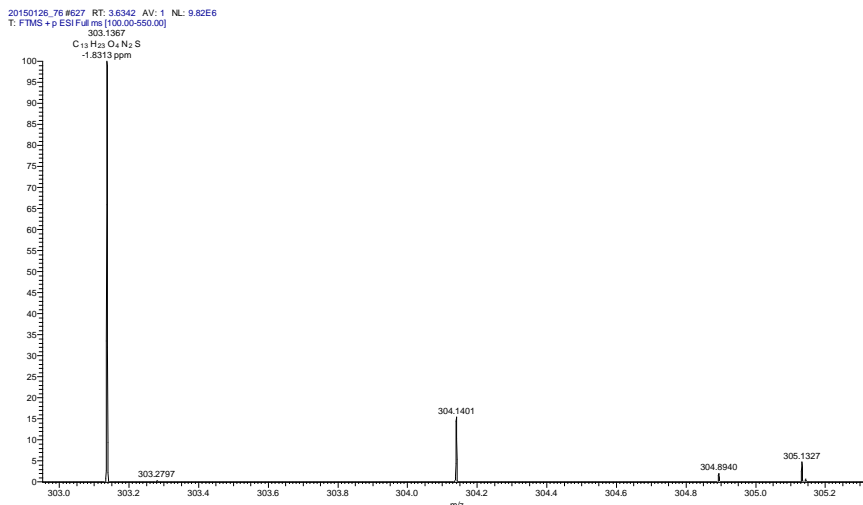

MS² Spectra
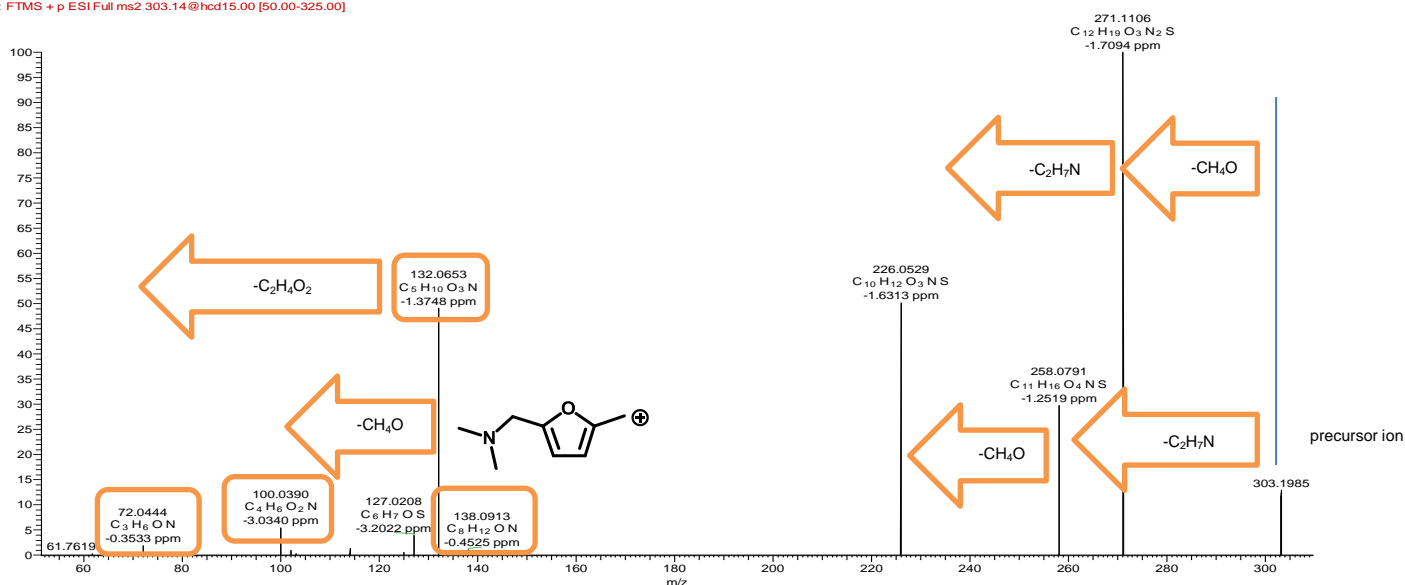
Formula

$C_{13}H_{22}N_2SO_4$

Atomic Modification

-2N +O

Proposed Structure
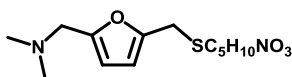
Confidence Level

Level 3
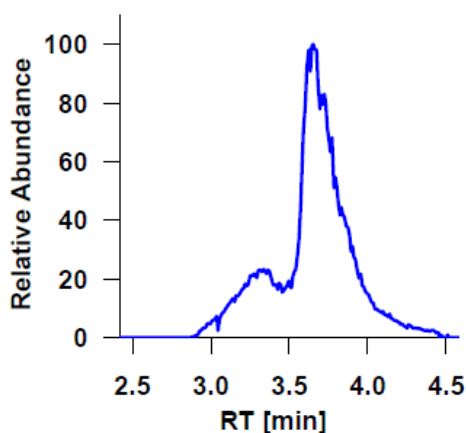TP class

Additional Evidence for Structure Interpretation

The MS² fragment at the nominal mass 138 as well as the neutral loss of C_2H_7N was observed for RAN as well as for RAN_TP_273.1263_3.2 and RAN_TP_289.1212_3.7, indicating that the substructure shown at nominal mass 138 is part of this TP. The MS² fragment at the nominal mass 132 indicates that the remaining atoms are connected. The structural evidence for this TP is similar to the one for RAN_TP_273.1263_3.2 and RAN_TP_289.1212_3.7, except that this TP consists of either an O atom or a CH_2O more and that a neutral loss of CH_4O can be observed multiple times. The occurrence of this neutral loss between the MS² fragments with the nominal mass 132 and 100 indicates that this moiety is present at the remaining, undefined part of the molecule. The MS² fragment at the nominal mass 72 most likely belongs to the undefined part of the molecule. The neutral loss between the MS² fragment at the nominal mass 132 and 72 is $C_2H_4O_2$. This indicates that the undefined part of $C_5H_{10}NO_3$ can be fragmented into two parts consisting of C_3H_6ON and $C_2H_4O_2$. The detailed structure of the remaining part, however, remains unknown.

**Attributed Reaction from the Parent Compound to this TP**

It was not possible to assign a reaction to this parent TP pair.

Figure S11. Structure elucidation of three RAN TP candidates identified from nontarget analysis.
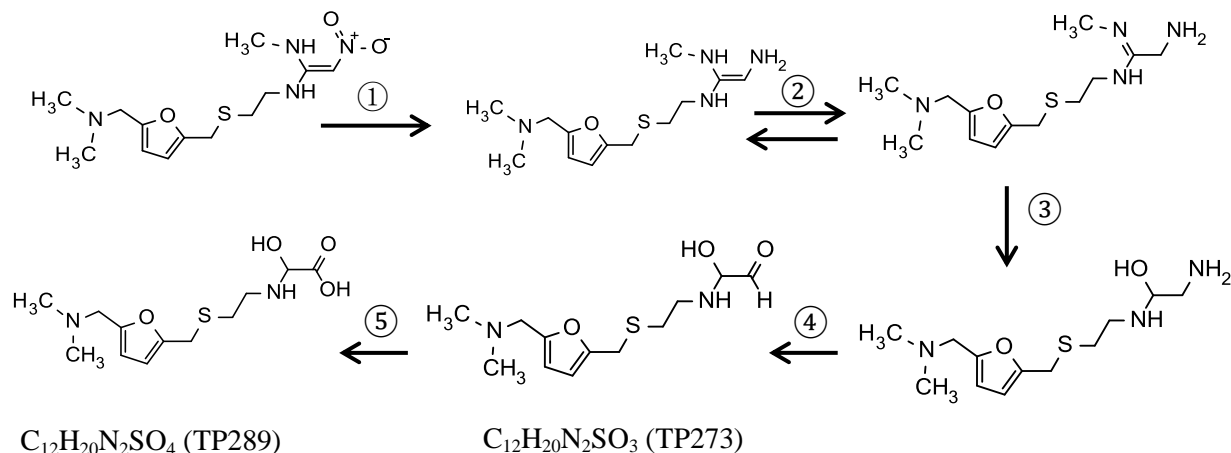
①: nitro reduction; ②: rearrangement; ③: hydrolysis; ④:deaminification; ⑤: oxidation

Figure S12 Hypothesized RAN biotransformation pathways.

S7 Proteomic analysis of *N. gargensis* during MIA and RAN biotransformation

Cell pellets were resuspended in 8 M urea/ 2 M thiourea buffer and sonicated (three cycles of

30 s, amplitude 0.7, power 70%) on-ice. After centrifugation, the pellets and the supernatant

were collected separately. The pellets were resuspended in solubilization buffer [1% (w/v)

Digitonin (AppliChem, Darmstadt, Germany), 300 mM NaCl, 100 mM Tris-HCl, pH 7.5] for

membrane protein extraction. The extracted membrane proteins combined with the previous

supernatant were precipitated using ice-cold acetone. The resulting protein pellets were subjected

to SDS-PAGE. Each sample lane was then cut into one gel band and prepared for proteolytic

cleavage. Protein lysate was reduced (2.5 mM DTT for 1 h at 60°C) and alkylated (10 mM

iodacetamide for 30 min at 37°C). Proteolysis was performed overnight using trypsin (Promega,

Madison, WI, USA) with an enzyme/substrate ratio of 1:25 at 37°C. Peptide lysates were

extracted from the gel and desalted using C_{18} ZipTips (Merck Millipore, Darmstadt, Germany).

The peptide lysates were separated on a UHPLC system (Ultimate 3000, Dionex/Thermo

Fisher Scientific, Idstein, Germany). Five µL samples were first loaded for 5 min on the

precolumn (µ-precolumn, cartridge column, 3 µm particle size, 75 µm inner diameter, 2 cm, C18,

Thermo Scientific) at 4% mobile phase B (80% acetonitrile in nanopure water with 0.08% formic acid), 96% mobile phase A (nanopure water with 0.1% formic acid), then eluted from the analytical column (PepMap Acclaim C_{18} LC Column, 25 cm, 3 μm particle size, Thermo Scientific) over a 120 min gradient of mobile phase B (4 – 55% B). Mass spectrometry was performed on an Orbitrap Fusion mass spectrometer (Thermo Fisher Scientific, Waltham, MA, USA) with a TriVersa NanoMate (Advion, Ltd., Harlow, UK) source in LC chip coupling mode. The MS was set on top speed with a cycle time of 3 s, using the Orbitrap analyzer for MS and MS/MS scans with higher energy collision dissoziation (HCD) fragmentation at normalized collision energy of 28%. MS scans were measured at a resolution of 120,000 in the scan range of 400 – 1600 *m/z*. MS ion count target was set to 4×10^5 at an injection time of 60 ms. Ions for MS/MS scans were isolated in the quadrupole with an isolation window of 2 Da and were measured with a resolution of 15,000 in the scan range of 350 – 1400 *m/z* in the Orbitrap. The dynamic exclusion duration was set to 30 s with a 10 ppm tolerance around the selected precursor and its isotopes. Automatic gain control target was set to 5×10^4 with an injection time of 120 ms.

Proteome Discoverer (v1.4.1.14, Thermo Scientific) was used for protein identification and the acquired MS/MS spectra were searched with the Sequest HT algorithm against the *N. gargensis* database (Uniprot/Swiss-Prot, containing 3,786 unreviewed sequence entries). For each individual search, we were able to assign an average of 767 distinct proteins with ≥ 1 peptide from 1,887 non-redundant peptides. Enzyme specificity was selected to trypsin with up to two missed cleavages allowed using 10 ppm peptide ion tolerance and 0.1 Da MS/MS tolerances. Oxidation (methionine) and carbamylation (lysine and arginine) were selected as a variable modifications and carbamidomethylation (cysteine) as a static modification. Only peptides with a false discovery rate (FDR) < 0.01 calculated by Percolator[6] and peptide rank = 1 were considered as identified.

The abundance of one detected protein was quantified using the average abundance of the top-3 peptide assigned to this protein. The abundance of all detected proteins in each sample was normalized to the abundance of a given protein. The significance of differential protein abundance was tested using the two-sample t-test on log10 values of the normalized protein abundances. T-tests were limited to proteins in which abundance of the protein was quantified in all three replicates in both control (ammonium as only substrate) and MP-treated samples. The multiple testing was subjected to Benjamini-Hochberg correction with FDR < 0.05. No protein-encoding gene was found to be statistically differentially expressed in the three MP-treated samples compared to the untreated one.

Partial least squares regression (PLS) was used to examine global differences of the normalized, log-transformed protein abundance profiles between the four groups (three MPs + ammonium, ammonium only) using the "plsr()" command from the "pls" library in R (Mevik and Wehrens, 2007).[7] Cluster significance was tested using label permutation and the Dunn index. Clustering by groups was found to show a trend but not statistically significant ($p = 0.107$). This is evidence that total protein profiles of *N. gargenesis* are not significantly different between the different treatments, consistent with the lack of differential expression of individual genes.

S8 Effects of the inhibitor PTIO on MIA and RAN biotransformation by nitrifying activated sludge from a Swiss municipal WWTP

The PTIO inhibition experiment was carried out in batch reactors with a reaction volume of 50 mL. Nitrifying activated sludge (NAS) was taken from the aeration tank in a Swiss municipal WWTP. The same ten MPs were first added into empty culture bottles in the same way as in the pure culture study. Right after being transported back to the lab, 50 mL of the freshly sampled NAS was inoculated into each of six reactors plated with ten MPs (final concentration 100 µg/L for each MP). PTIO was then added into three reactors (final concentration 100 µM), the other

three reactors without PTIO served as control. All reactors were then loosely capped with cotton stopper, and incubated with shaking at 160 rpm. After letting the plated MPs re-dissolve for 30 min, 1.5 mL sludge sample was taken as 0 h sample. The sludge sample was then centrifuged at 13,000 rpm, room temperature for 10 min. The supernatant was transferred into a 2 mL amber glass HPLC vial and stored at 4 °C in dark till LC-MS/MS analysis (max. 10-day storage before analysis). Compound concentrations were analyzed by reversed phase liquid chromatography coupled to a high-resolution quadrupole orbitrap mass spectrometer (LC-MS/MS) (QExactive, Thermo Fisher Scientific Corporation, San Jose, US). Samples were loaded directly onto an XBridge C_{18} column (particle size 3.5 μm, 2.1 × 50 mm, Waters). The MS detection was done by full scan acquisition (resolution of 140,000 at 200 *m/z*, a range of 50 – 750 *m/z*) followed by three data-dependent MS/MS scans (resolution of 17,500 at 200 *m/z*). Calibration curves were established using matrix-matched standard series ranging between 10 and 750 ng/L in 20mL. The lowest calibration point of 10 ng/L was regarded as the limit of quantification (LOQ). Only the biotransformation and TP formation of MIA and RAN out of the ten MPs were inhibited by PTIO, consistent with the compound specificity of the AOA pure culture, *N. gargensis*. Notably, the ammonia oxidation was not inhibited by PTIO, indicating that the ammonia oxidation was carried out by AOB. The AOA/AEA groups, if present, might be at low abundance in the tested NAS community, hence have trivial contribution to ammonia oxidation. This may also explain the small degree of inhibition on MIA and RAN biotransformation by PTIO.
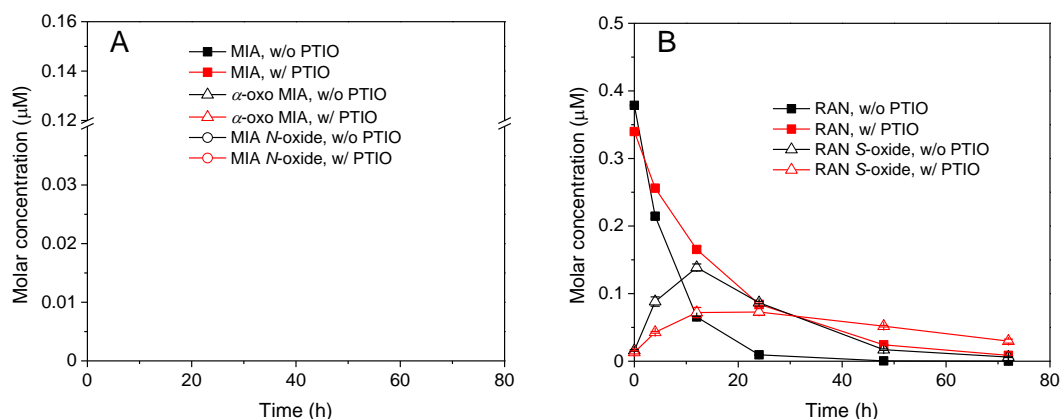
Figure S13. Biotransformation and TP formation of MIA (A) and RAN (B) by NAS with and without the addition of PTIO.

Albeit in low abundance, AOA/AEA were likely present in the NAS community analyzed, as i) archaeal *amoA* gene transcripts were detected previously from the sludge of the same WWTP by reverse transcription quantitative PCR (RT-qPCR)[4]; ii) fourteen metatranscriptomic sequencing reads (0.004%) were aligned with *Thaumarchaeota* by MG-RAST (with an average e value of $10^{-9.75}$, an average identity of 69%, MG-RAST ID: 4491748.3, unpublished data); iii) despite of some unspecific amplification, a PCR product with the expected size (~440 bp) was obtained from genomic DNA of the analyzed NAS, using *Thaumarchaeota*-specific primers (Thaum494/Arc917R) targeting the 16S rRNA gene [8] The sample used for the experiments described under i) and ii) was taken in March 2011, and the one used in iii) was taken 8 month ahead of the PTIO inhibition experiment from the same WWTP. To our knowledge, no substantial constructional disturbance occurred to the WWTP during the entire sampling time course.

References

(1) Huntscha, S.; Singer, H. P.; McArdell, C. S.; Frank, C. E.; Hollender, J., Multiresidue analysis of 88 polar organic micropollutants in ground, surface and wastewater using online mixed-bed multilayer solid-phase extraction coupled to high performance liquid chromatography-tandem mass spectrometry. *J. Chromatogr. A* **2012**, *1268*, 74–83.

(2) Ely, R. L.; Williamson, K. J.; Hyman, M. R.; Arp, D. J., Cometabolism of chlorinated solvents by nitrifying bacteria: kinetics, substrate interactions, toxicity effects, and bacterial response. *Biotechnol. Bioeng.* **1997,** *54*, 520–534.

(3) Liu, L.; Binning, P. J.; Smets, B. F., Evaluating alternate biokinetic models for trace pollutant cometabolism. *Environ. Sci. Technol.* **2015,** *49*, 2230–2236.

(4) Helbling, D. E.; Johnson, D. R.; Honti, M.; Fenner, K., Micropollutant biotransformation kinetics associate with WWTP process parameters and microbial community characteristics. *Environ. Sci. Technol.* **2012,** *46*, 10579–10588.

(5) Gulde, R.; Helbling, D. E.; Scheidegger, A.; Fenner, K., pH-dependent biotransformation of ionizable organic micropollutants in activated sludge. *Environ. Sci. Technol.* **2014,** *48*, 13760–13768.

(6) Kall, L.; Canterbury, J. D.; Weston, J.; Noble, W. S.; MacCoss, M. J., Semi-supervised learning for peptide identification from shotgun proteomics datasets. *Nat. Methods* **2007,** *4*, 923–925.

(7) Mevik, B. H.; Wehrens, R., The pls package: Principal component and partial least squares regression in R. *J. Stat. Softw.* **2007,** *18*, 1–23.

(8) Hong, J. K.; Kim, H. J.; Cho, J. C., Novel PCR primers for the archaeal phylum Thaumarchaeota designed based on the comparative analysis of 16S rRNA gene sequences. *PloS one* **2014,** *9*, e96197.